Supporting Information

2D/3D Heterostructured $CsPbI_2Br$ Solar Cells: A Choice for a Monolithic All-perovskite Tandem Device

Liqiu Yan[a], Yan Li[a], Siqi Li[a], Xiangnan Sun[a], Yao Li[a], Xue Han[b], Meilan Huang[c], Xia Tao[a,*]

a State Key Laboratory of Organic-Inorganic Composites, Beijing University of Chemical Technology, Beijing 100029, China

b Department of Chemical Engineering, Virginia Polytechnic Institute and State University, Blacksburg, Virginia 24061, United States

c School of Chemistry & Chemical Engineering, Queen's University Belfast, Belfast, BT9 5AG, UK

* Corresponding author. Tel: +86-10-6445-3680 Fax: +86-10-6443-4784

E-mail: taoxia@mail.buct.edu.cn

Experimental section

Materials: Cesium iodide (CsI, 99.999%), lead bromide ($PbBr_2$, 99.999%), lead iodide (PbI_2, 99.999%), n-butylammonium bromide (BABr, 99.5%), methylazanium iodide (MAI, 99.9%), PEDOT:PSS (PH1000, 1.0~1.3 wt%), Fullerene (C_{60}, 99%), Spiro-OMeTAD and Tris (2- (1H-pyrazol-1-yl)-4-tert-butylpyridine)-cobalt (III)Tris (bis- (trifluoromethyl sulfonyl) imide)) (FK209) were purchased from Xi'an Polymer Light Technology Corp. SnO_2 colloid precursor (15 wt% in H_2O colloidal dispersion) was purchased from Alfa Aesar. Dimethyl sulfoxide (DMSO, 99.8%), isopropanol (IPA, 99.5%), chlorobenzene (CB, 99.9%), acetonitrile (ACN, 99.8%), Li-TFSI (99.95%), and TBP (4-tert-butylpyridine, 96%) were purchased from Sigma-Aldrich. All materials were used without further purification.

Perovskite Film Characterization:

XRD: The crystal structure of perovskite layers with different treatment concentrations were examined by X-ray diffractometer (XRD) (Bruker Metrology Nanoscope III-D) with Cu Kα radiation (λ = 1.5418 Å) operated at 30 mA and 40 kV. The XRD data were taken from unfinished devices on the same layer sequence as the perovskite solar cell, but excluding the Ag electrode and the Spiro-OMeTAD HTL.

SEM: High-resolution field emission cross-sectional and top-view scanning electron microscope (SEM) images of $CsPbI_2Br$ perovskite films with the different treatment concentrations of 0, 0.1, 0.5, 1, and 3 mg mL^{-1} BABr solution were taken with a scanning electron microscope (S4700) with an in-lens detector and an aperture size of 20 μm.

AFM: Atomic Force Microscope (AFM) is used to test the surface roughness of samples, the model used is the German Bruker-Fastscan. The principle is to show the three-dimensional morphology according to the different forces on the surface area of the sample, and finally calculate its mean square value. The film sample prepared in the experiment has a scanning area of 4 μm^2 and a resolution of 256×256 Hz.

UV-vis: Ultraviolet-visible (UV-vis) absorption spectra were recorded using a UV-vis-NIR spectrophotometer (Lambda 950, PerkinElmer, USA) in the 300-800 nm wavelength range at room temperature. In addition, the device can also test the transmittance of the electron transport layer to ultraviolet and visible light.

PL and TRPL: The steady-state photoluminescence (PL) spectrum (FLS920, Edinburgh Instruments, U.K.) was first used in the experiment, the excitation wavelength was set to 460 nm, and the scanning wavelength was 600-750 nm. Secondly, transient photoluminescence (TRPL) spectroscopy is used, it was measured on a photoluminescent spectrometer (FLS 980, Edinburgh Instruments), excited with a picosecond pulsed diode laser CW NIR laser at 470 nm as the excitation source.

XPS and UPS: The X-ray photoelectron spectroscopy (XPS) (Thermo Scientific K-Alpha+) measurement is used to test the change of spectral peak, XPS were determined suitable to avoid an influence of beam-induced changes on the spectra. Ultraviolet photoelectron spectroscopy (UPS) measurement (Thermo ESCALAB XI+) is used to test the change of work function and energy level.

Raman: Raman spectra were measured using a microspectroscopic Raman setup to analyze the molecular structure and composition changes (Raman-HR-TEC-405).

Device Characterization:

J-V: Photovoltaic performance of PSCs was characterized by measuring the current density-voltage (*J-V*) curve under AM 1.5G sunlight with 100 mW cm^{-2} light output using a solar light simulator (Newport Oriel Sol 3A class, US, calibrated by a Newport reference cell), and the data were recorded with a Keithley 2400 source meter from 1.5 V to -0.5 V with a scan rate of 0.2 V s^{-1} and a pre-condition of 0.5 s. The cell size was 1.5×1.5 cm, and the active area of each solar cell was 0.04 cm^2, which was defined by the area of the Ag electrode.

EQE: Also known as IPCE, EQE was acquired by an Oriel QEPVSI system equipped with a 300 W Xe lamp for irradiation together with a calibrated silicon photodetector.

M-S: The Mott-Schottky test is an important method to explain the charge recombination mechanism. It was performed on the Zennium electrochemical workstation at 10 kHz frequency under dark condition.

EIS: Electrochemical impedance spectra (EIS) was recorded using a Zahner system of the Zennium electrochemical workstation under dark conditions and illuminated under AM 1.5G sunlight with a bias of 0.8 V, with frequencies ranging from 10 Hz to 1 M Hz and a modulation amplitude of 10 mV.

SCLC: Space-charge-limited Current (SCLC) test was measured at room temperature under dark conditions to characterize the defect state density of perovskite thin films in pure electronic devices.

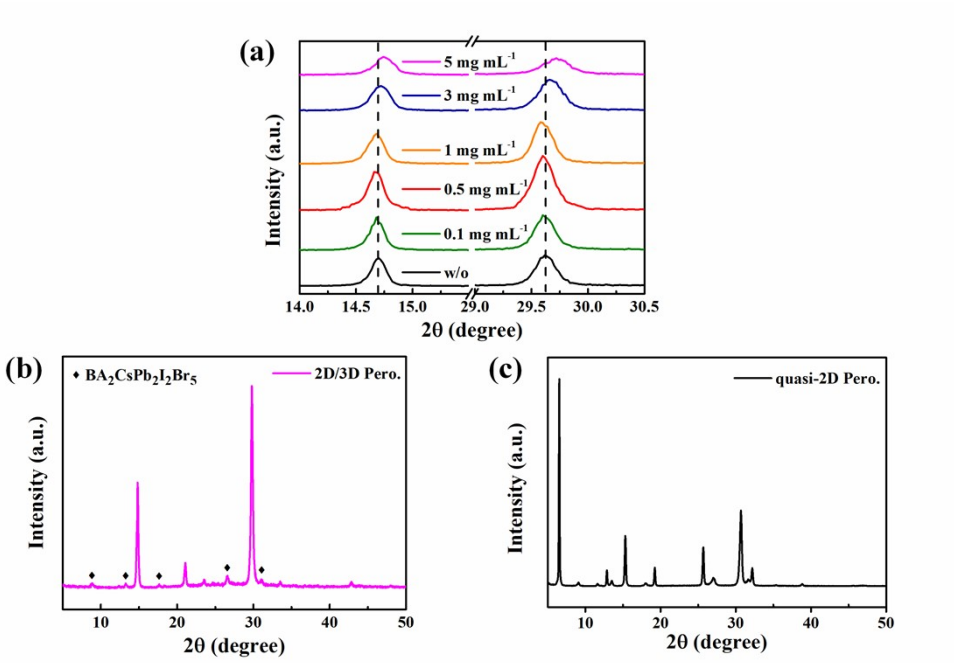

Fig. S1 (a) Magnification of XRD patterns at (100) and (200) planes, XRD patterns of (b) 5 mg mL^{-1} BABr treated $CsPbI_2Br$ and (c) $BA_2CsPb_2I_2Br_5$ films.

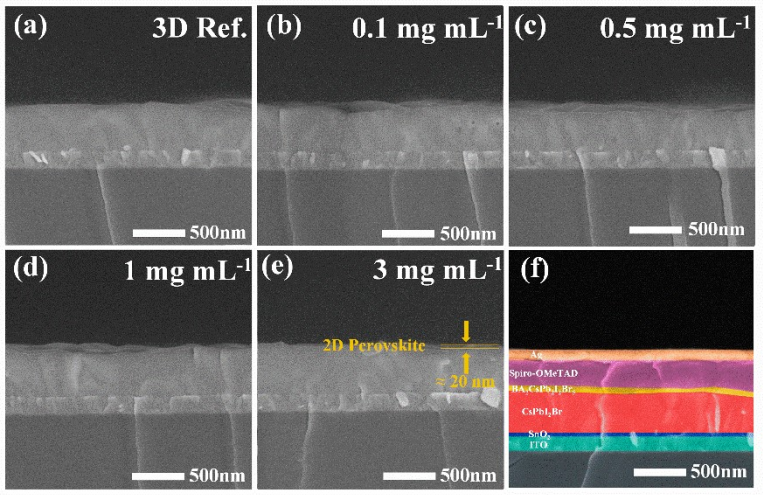

Fig. S2 Cross-sectional SEM images of the $CsPbI_2Br$ samples modified with different concentrations of BABr: (a) 0 mg mL^{-1}, (b) 0.1 mg mL^{-1}, (c&f) 0.5 mg mL^{-1} and (d) 1 mg mL^{-1} and (e) 3 mg mL^{-1}.

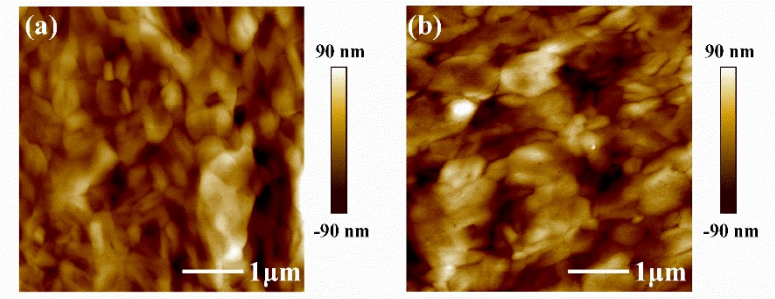

Fig. S3 Top-view AFM images of the (a) pristine and (b) 2D/3D perovskite films with 0.5 mg mL^{-1} BABr.

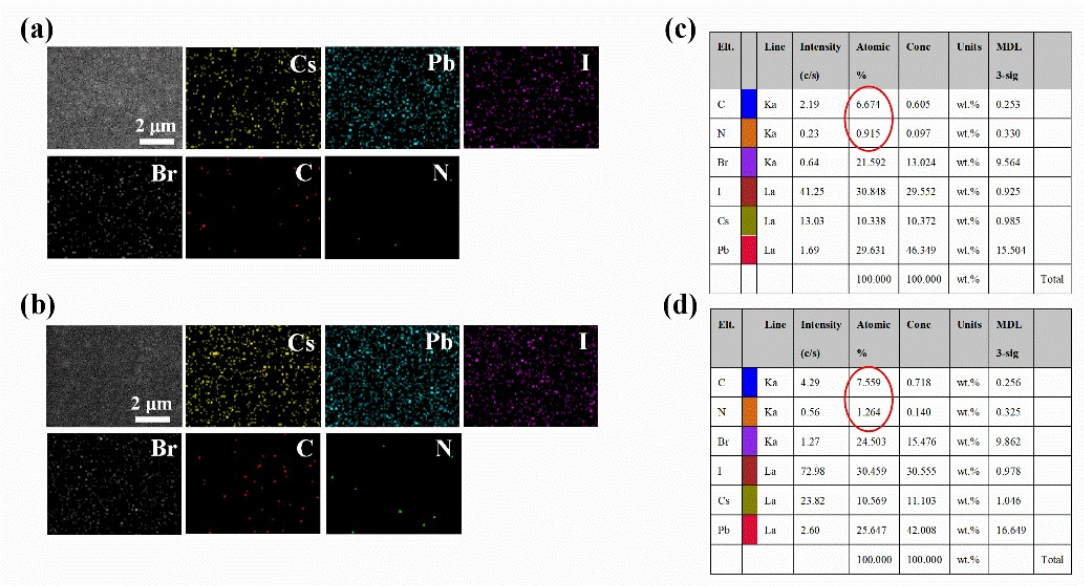

(c)

Elt.		Line	Intensity (c/s)	Atomic %	Conc	Units	MDL 3-sig	
C		Ka	2.19	6.671	0.605	wt.%	0.253	
N		Ka	0.23	0.915	0.097	wt.%	0.330	
Br		Ka	0.64	21.592	13.024	wt.%	9.564	
I		La	41.25	30.848	29.552	wt.%	0.925	
Cs		La	13.03	10.338	10.372	wt.%	0.985	
Pb		La	1.69	29.631	46.349	wt.%	15.501	
				100.000	100.000	wt.%		Total

(d)

Elt.		Line	Intensity (c/s)	Atomic %	Conc	Units	MDL 3-sig	
C		Ka	4.29	7.559	0.718	wt.%	0.256	
N		Ka	0.56	1.264	0.140	wt.%	0.325	
Br		Ka	1.27	24.503	15.476	wt.%	9.862	
I		La	72.98	30.459	30.555	wt.%	0.978	
Cs		La	23.82	10.569	11.103	wt.%	1.046	
Pb		La	2.60	25.647	42.008	wt.%	16.649	
				100.000	100.000	wt.%		Total

Fig. S4 SEM and EDS mappings of (a) pristine and (b) 2D/3D perovskite films with 0.5 mg mL^{-1} BABr and (c&d) the percentage of element content in the control group and the optimized group.

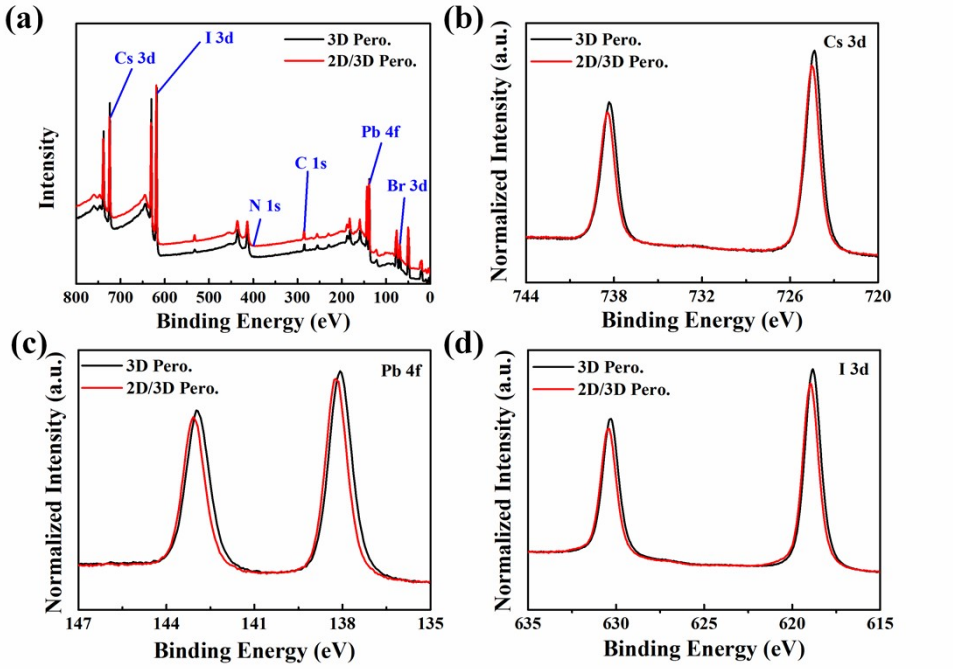

Fig. S5 XPS of (a) $CsPbI_2Br$, (b) Cs 3d, (c) Pb 4f and (d) I 3d of the 3D $CsPbI_2Br$ (black) and the 2D/3D perovskite films (red) treated with 0.5 mg mL^{-1} BABr.

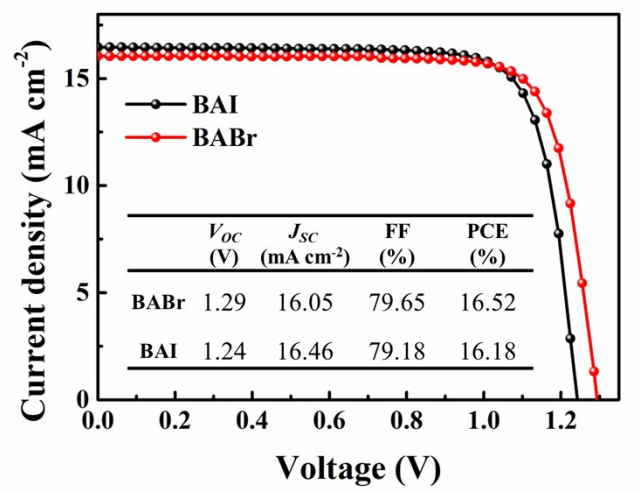

Fig. S6 *J-V* curves of optimized devices with BABr and BAI treated $CsPbI_2Br$.

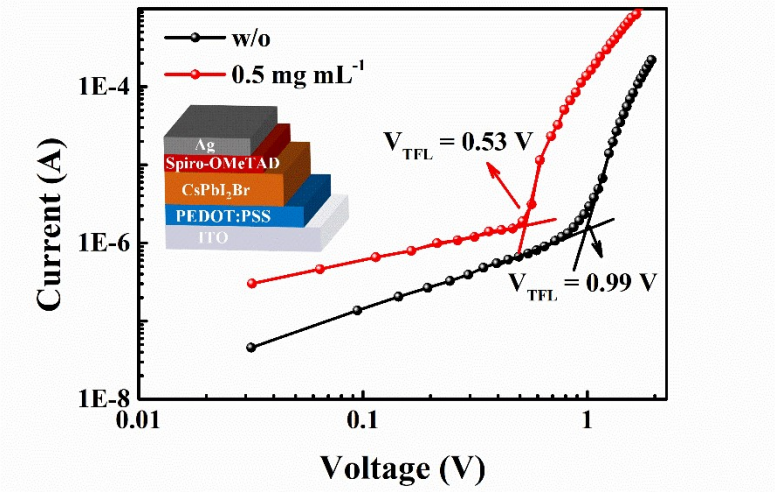

Fig. S7 Dark J-V curves for the hole-only devices with the structure of glass/ITO/PEDOT:PSS/2D/3D $CsPbI_2Br$ (or 3D $CsPbI_2Br$)/Spiro-OMeTAD/Ag.

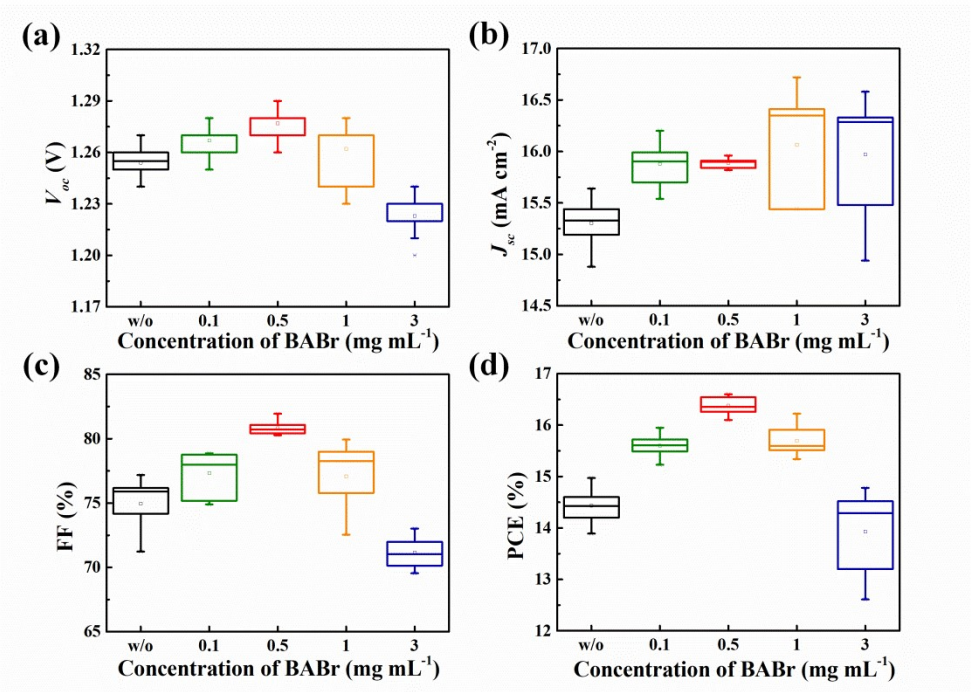

Fig. S8 (a) V_{oc}, (b) J_{sc}, (c) FF and (d) PCE distributions of pristine device and optimized devices with different concentrations of BABr.

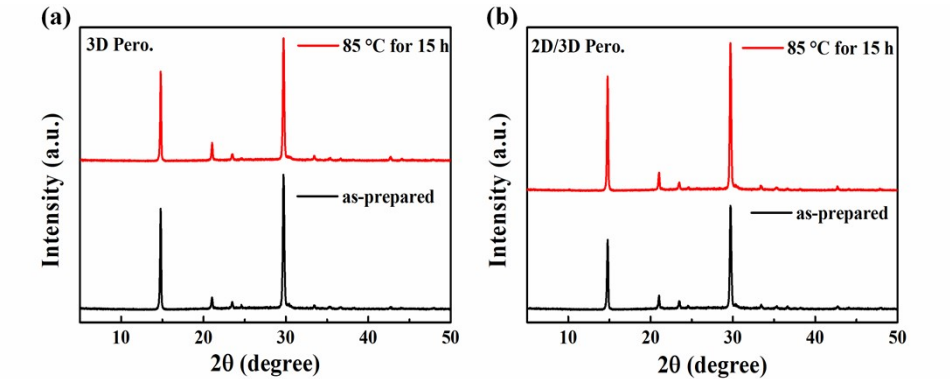

Fig. S9 XRD patterns of (a) 3D $CsPbI_2Br$ film and (b) 2D/3D $CsPbI_2Br$ film with and without heating at 85 ºC for 15 hours in a N_2 atmosphere.

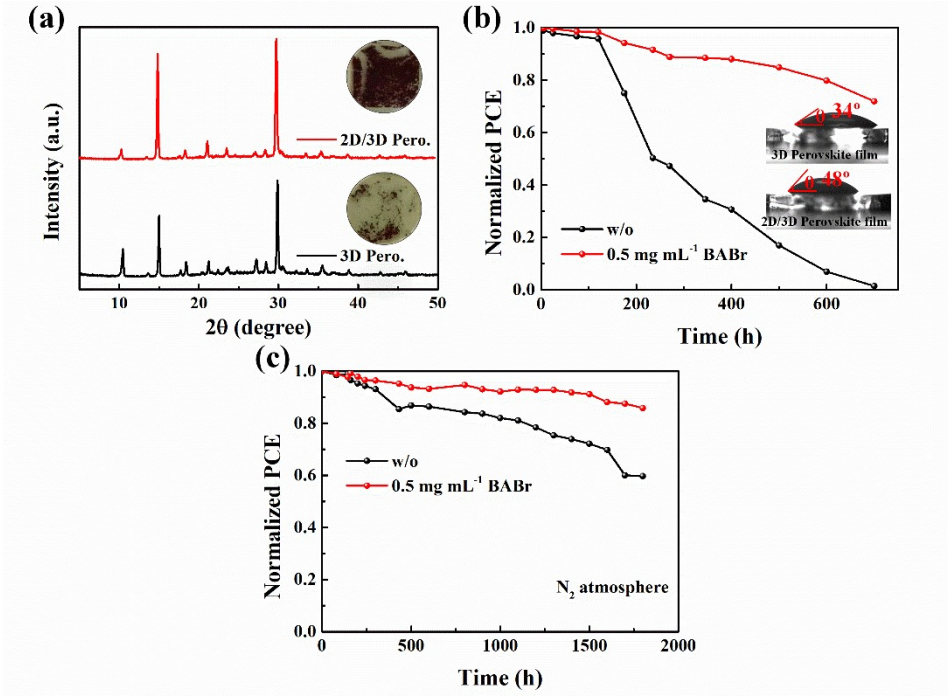

Fig. S10 (a) XRD patterns of 3D $CsPbI_2Br$ and 2D/3D $CsPbI_2Br$ films after being placed in the environment (60% RH) for 10 min (the inset is the optical photos of the perovskite films). (b) Moisture stability of the devices aged at the controlled 25% RH ambient condition (the inset is the contact angle of the perovskite films by utilizing water as the test solvent) and (c) the long-term stability of pristine and optimal devices stored in a N_2 atmosphere.

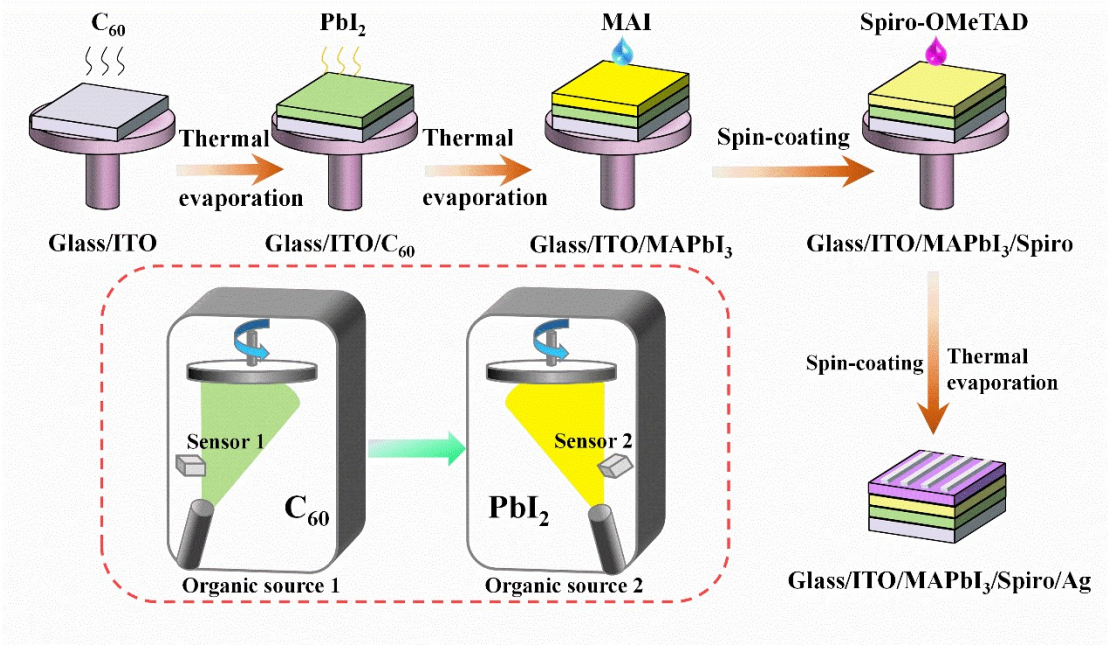

Fig. S11 Fabrication process of $MAPbI_3$ PSCs.

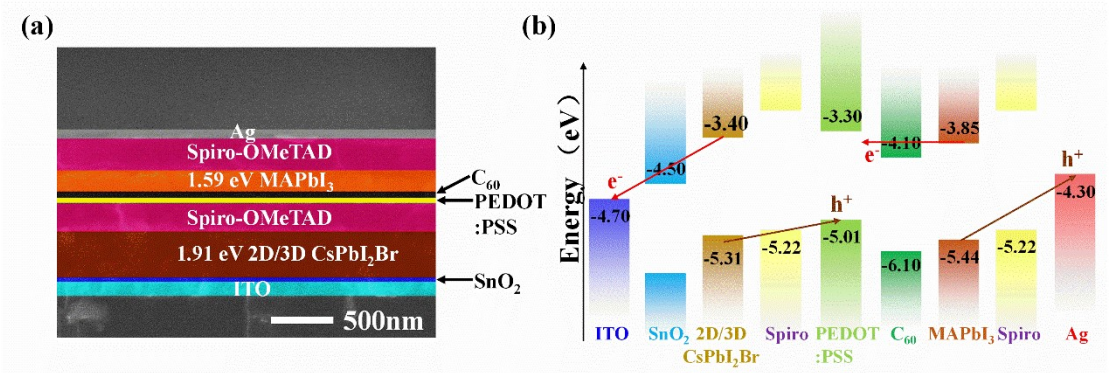

Fig. S12 (a) Cross-sectional SEM and (b) energy band diagram of the monolithic all-PTSC.

Table S1 Fitting parameters of the TRPL decay spectra for $CsPbI_2Br$ films with different concentrations of BABr.

BABr (mg mL^{-1})	**τ_1 (ns)**	**τ_2 (ns)**	**Average (τ) (ns)**
w/o	5.92	15.22	12.99
0.1	6.65	17.71	13.67
0.5	4.97	13.50	11.36
1	2.09	10.24	6.30
3	0.49	2.47	0.71

Table S2 Comparison of photovoltaic performance parameters of $CsPbI_2Br$ PSCs without modification.

Device Structure	Perovskite dimension	V_{OC} (V)	J_{SC} (mA cm^{-2})	FF (%)	PCE (%)	Ref.
ITO/SnO_x/$CsPbI_2Br$/poly (DTSTPD-r-BThTPD)/Au	3D	1.24	13.48	75.00	12.54	1
ITO/SnO_2/TiO_2/$CsPbI_2Br$/Spiro/MoO_3/Ag	3D	1.19	15.47	75.26	13.85	2
FTO/ZnO@SnO_2/$CsPbI_2Br$/Spiro/MoO_3/Ag	3D	1.03	16.34	69.00	11.66	3
ITO/SnO_2/PN4N/$CsPbI_2Br$/PDCBT/MoO_3/Ag	3D	1.08	14.8	76.70	12.30	4
ITO/SnO_2/$CsPbI_2Br$/CsBr/Spiro/Au	3D	1.10	16.17	66.68	11.81	5
ITO/Im-SnO_2/$CsPbI_2Br$/Spiro/Au	3D	1.20	15.44	76.15	14.11	6
ITO/ZnO/SnO_2/$CsPbI_2Br$/ (PEABr+ CsBr)/Spiro/Ag	3D	1.23	15.4	74.00	14.00	7
ITO/ZnO-SnO_2/SC-$CsPbI_2Br$/Spiro/Ag	3D	1.25	15.10	75.11	14.45	8
ITO/SnO_2/$CsPbI_2Br$/Spiro/Ag	2D/3D	1.06	15.96	81.50	13.70	9
ITO/SnO_2/$CsPbI_2Br$/Spiro/Ag	2D/3D	1.25	15.61	75.71	14.78	This work

Table S3 Comparison of photovoltaic performance parameters of "champion" $CsPbI_2Br$ PSCs.

Device Structure	Perovskite dimension	V_{OC} (V)	J_{SC} (mA cm^{-2})	FF (%)	PCE (%)	Ref.
ITO/SnO_x/$CsPbI_2Br$/poly (DTSTPD-r-BThTPD)/Au	3D	1.41	14.25	77.00	15.53	1
ITO/SnO_2/TiO_2/$CsPbI_2Br$/Spiro/MoO_3/Ag	3D	1.23	15.67	82.29	15.86	2
FTO/ZnO@SnO_2/$CsPbI_2Br$/Spiro/MoO_3/Ag	3D	1.11	16.45	79.00	14.35	3
ITO/SnO_2/PN4N/$CsPbI_2Br$/PDCBT/MoO_3/Ag	3D	1.30	15.30	81.50	16.20	4
ITO/SnO_2/$CsPbI_2Br$/CsBr/Spiro/Au	3D	1.27	16.72	77.18	16.37	5
ITO/Im-SnO_2/$CsPbI_2Br$/Spiro/Au	3D	1.31	15.53	79.13	16.10	6
ITO/ZnO/SnO_2/$CsPbI_2Br$/ (PEABr+ CsBr)/Spiro/Ag	3D	1.30	15.64	82.00	16.70	7
ITO/ZnO-SnO_2/SC-$CsPbI_2Br$/Spiro/Ag	3D	1.31	15.90	81.48	16.97	8
ITO/SnO_2/$CsPbI_2Br$/Spiro/Ag (BAI)	2D/3D	1.08	16.80	80.10	14.50	9
ITO/SnO_2/$CsPbI_2Br$/Spiro/Ag (BABr)	2D/3D	1.28	15.92	81.35	16.57	This work

Table S4 Comparison of configuration and photovoltaic performance parameters of monolithic all-perovskite tandem solar cells.

Sub cells	Absorbers	Recombination layer	V_{oc} (V)	J_{sc} (mA cm^{-2})	FF	PCE (%)	Ref.
Top Bottom	$MAPbI_3$ (1.55 eV) $MAPbI_3$ (1.55 eV)	PEDOT:PSS	1.89	6.61	56.00	7.00	10
Top Bottom	$MAPbBr_3$ (2.30 eV) $MAPbI_3$ (1.55 eV)	PEDOT:PSS	1.96	6.40	41.00	5.10	11
Top Bottom	2D/3D $CsPbI_2Br$ (1.91 eV) $MAPbI_3$ (1.55 eV)	PEDOT:PSS	2.33	8.04	54.54	10.22	This work

References

1. Z. Guo, A. K. Jena, I. Takei, G. M. Kim, M. A. Kamarudin, Y. Sanehira, A. Ishii, Y. Numata, S. Hayase and T. Miyasaka, *J. Am. Chem. Soc.*, 2020, **142**, 9725-9734.
2. Y. Wang, C. Duan, X. Zhang, N. Rujisamphan, Y. Liu, Y. Li, J. Yuan and W. Ma, *ACS Appl. Mater. Interfaces*, 2020, **12**, 31659-31666.
3. Z. Li, R. Wang, J. Xue, X. Xing, C. Yu, T. Huang, J. Chu, K.-L. Wang, C. Dong, Z. Wei, Y. Zhao, Z.-K. Wang and Y. Yang, *J. Am. Chem. Soc.*, 2019, **141**, 17610-17616.
4. J. Tian, Q. Xue, X. Tang, Y. Chen, N. Li, Z. Hu, T. Shi, X. Wang, F. Huang, C. J. Brabec, H.-L. Yip and Y. Cao, *Adv. Mater.*, 2019, **31**, 1901152.
5. Y. Zhang, C. Wu, D. Wang, Z. Zhang, X. Qi, N. Zhu, G. Liu, X. Li, H. Hu, Z. Chen, L. Xiao and B. Qu, *Sol. RRL*, 2019, **3**, 1900254.
6. S. Liu, W. Chen, Y. Shen, S. Wang, M. Zhang, Y. Li and Y. Li, *J. Mater. Chem. A*, 2020, **8**, 14555-14565.
7. J. He, J. Su, Z. Lin, J. Ma, L. Zhou, S. Zhang, S. Liu, J. Chang and Y. Hao, *Adv. Sci.*, 2021, **8**, 2101367.
8. J. Ma, Z. Lin, X. Guo, L. Zhou, J. He, Z. Yang, J. Zhang, Y. Hao, S. Liu and J. Chang, *J. Energy Chem.*, 2021, **63**, 558-565.
9. M. Tai, Y. Zhou, X. Yin, J. Han, Q. Zhang, Y. Zhou and H. Lin, *J. Mater. Chem. A*, 2019, **7**, 22675-22682.
10. F. Jiang, T. Liu, B. Luo, J. Tong, F. Qin, S. Xiong, Z. Li and Y. Zhou, *J.*

Mater. Chem. A, 2016, **4**, 1208-1213.

11. R. Sheng, M. T. Hörantner, Z. Wang, Y. Jiang, W. Zhang, A. Agosti, S. Huang, X. Hao, A. Ho-Baillie, M. Green and H. J. Snaith, *J. Phys. Chem. C*, 2017, **121**, 27256-27262.